Temperature behaviour of the structural, magnetic and vibrational properties of $KGd(WO_4)_2$ single crystal

L. Macalik[a] , S. M. Kaczmarek[b,*], G. Leniec[b], J. Hanuza[a], A. Pietraszko[a], T. Bodziony[b], T. Skibiński[b]

[a] *Institute of Low Temperature and Structure Research PAS, Okólna 2, 50-422 Wrocław, Poland*
[b] *Institute of Physics, West Pomeranian University of Technology, Al. Piastów 48, 70-311 Szczecin, Poland*

[*] *Author for correspondence: S. M. Kaczmarek, email: Slawomir.Kaczmarek@zut.edu.pl*
Received 28 Apr 2014; Accepted 01 Jul 2014; Available Online 01 Jul 2014

Abstract

Crystal structure, magnetic and vibrational properties of $KGd(WO_4)_2$ single crystal in dependence on temperature were studied. Electron paramagnetic resonance (EPR) and Raman spectroscopy as well as crystallographic measurements were used. Results of the Raman and crystallographic measurements do not point out any structural transition up to 4 K. The EPR spectra of $KGd(WO_4)_2$ single crystal recorded in ***ab***, ***bc*** and ***ac*** planes in temperature range 8-300 K are broad and reveal a complex shape. Detailed analysis suggests contribution of several magnetically inequivalent paramagnetic centres. Temperature dependences of EPR resonance lines positions, linewidths and anisotropy factor as well as angular dependences were measured and calculated taking into account superposition of three at least different lines. The dependences reveal two temperatures at which a behaviour of the total intensity suddenly changes: ~67 K and ~10 K. We assigned them to a change in a kind of dominating magnetic interactions or activity of different magnetic systems, e.g. inter-chains, intra-chains and pairs or clusters.

Keywords: Double tungstate; Electron paramagnetic resonance; Magnetic systems; Raman spectroscopy; Crystallographic parameters

1. Introduction

Single crystals of $KGd(WO_4)_2$ double tungstate (thereafter KGW) are still in focus of attention as an effective laser medium with a low generation threshold. The monoclinic KGW crystal is a good laser host, easy for doping with large concentration of rare earth ions. That provides high efficiency for stimulated emission at low pumping energies, both with lamp and laser diode excitation [1, 2]. $KY(WO_4)_2$ and $KGd(WO_4)_2$ were known as very efficient and promising hosts for the Nd^{3+} ion at intermediate power levels for long time. Application of KGW:Nd^{3+} laser crystal as an active SRS (Stimulated Raman Scattering) element was one of contribution to development of compact solid state Raman laser for near infrared and eye safe spectral region of about 1.5 μm [3-6]. KGW single crystals doped with rare-earth elements like neodymium (Nd^{3+}) or erbium (Er^{3+}) could be applied in long-distance optical communicators [7, 8].

In this paper, we report X-ray diffraction, Raman and EPR studies of monoclinic $KGd(WO_4)_2$ single crystal. EPR data testify that at low temperature, certain behaviour different from the usual, could appear. Verification of the structural and Raman measurements with the decrease of temperature was necessary. The aim of these studies is to gain information on the temperature influence on structural and vibrational properties of potassium gadolinium double tungstate and possible structural changes in KGW.

2. Experimental Details

KGW single crystals were grown by a low-gradient Czochralski technique (modified top-seeded solution method) in platinum crucibles using oriented seeds along the crystallographic *b* axis [7]. Orientation of the crystals was done by X-ray method giving *a*, *b* and *c* axes directions.

The X-ray diffraction data (thereafter XRD) were collected at the room temperature (RT) and 11 K using an automatic X-ray four-circle "X'Calibur" diffractometer (Oxford Diffraction Company) with CCD area detectors and the low temperature attachment "HeliJet". The stability of the temperature of the stream of gaseous helium was carried out about ±1°. Graphite monochromatic Mo-K_α radiation (λ = 0.071073 nm) was generated at 50 kV and 25 mA. A single image for 1.2° rotation around the ω axis was obtained during 20 s and the full set of X-ray diffraction in the 2θ angle was collected over the range from 3 to 58.22° at 11 K (40 s and 2θ = 59.33° at RT). The intensities of the reflections were recorded in 117 frames at 11 K (742 frames at RT). Data reduction was performing using the CrysAlis version 172.33.42 Oxford Diffraction system with analytic absorption correction. The crystal structures were redeterminated, using as the initial atomic coordinates, determined by Pujol et al. [8] and using program [Shelxs99] [9]. The basic crystallographic data and the details of the measurement and refinement are summarized in Table 1.

EPR spectra were recorded on a conventional X-band Bruker ELEXSYS E 500 CW-spectrometer operating at 9.5 GHz with 100 kHz magnetic field modulation. Temperature dependence of the EPR spectra from 4 K to room temperature was recorded using an Oxford Instruments ESP nitrogen-flow cryostat.

The polarized Raman spectra were measured using a Bruker FT 100/S spectrometer. Measurements were performed in back scattering geometry onto the face perpendicular to

Table 1. Crystal data and structure refinement for $KGd(WO_4)_2$ at RT and 11 K.

Empirical formula	Gd K O_8 W_2	Gd K O_8 W_2
Formula weight	692.05	692.05
Temperature (K)	11(2)	293(2)
Wavelength (Å)	0.71073	0.71073
Crystal system, space group	Monoclinic, C2/c	Monoclinic, C2/c
Unit cell dimensions (Å):		
a	10.683(2)	10.6937(13)
b	10.452(2)	10.4427(6)
c	7.583(2)	7.6037(10)
α (deg)	90	90
β (deg)	130.70(3)	130.79(2)
γ (deg)	90	90
Volume (Å^3)	641.9(2)	642.91(12)
Z, Calculated density (Mg m^{-3})	4, 7.161	4, 7.150
Absorption coefficient (mm^{-1})	46.615	46.544
F(000)	1180	1180
Crystal size (mm)	0.17 x 0.15 x 0.12	0.17 x 0.15 x 0.12
Θ range for data collection (deg)	3.18 – 29.11	3.18 – 29.66
Limiting indices	$-14 \le h \le 9$, $-14 \le k \le 5$, $0 \le l \le 10$	$-14 \le h \le 13$, $-14 \le k \le 12$, $-10 \le l \le 9$
Reflections collected/unique	739/620 (R_{int} = 0.0145)	3811/864 (R_{int} = 0.0343)
Completeness to Θ = 29.11	70.9 %	94.3 %
Absorption correction	Spherical -CrysAlis v-171	
Refinement method	Full-matrix least-squares on F^2	
Data/restraints/parameters	620/0/57	864/0/57
Goodness-of-fit on F^2	1.758	1.231
Final *R* indices [I > 2σ(I)]	R_1 = 0.0593, wR_2 = 0.1478	R_1 = 0.0218, wR_2 = 0.0516
R indices (all data)	R_1 = 0.0627, wR_2 = 0.1486	R_1 = 0.0243, wR_2 = 0.0522
Extinction coefficient	0.00281(6)	0.0134(2)
Largest diff. peak and hole (e Å^{-3})	5.037 and -4.933	2.291 and -1.811

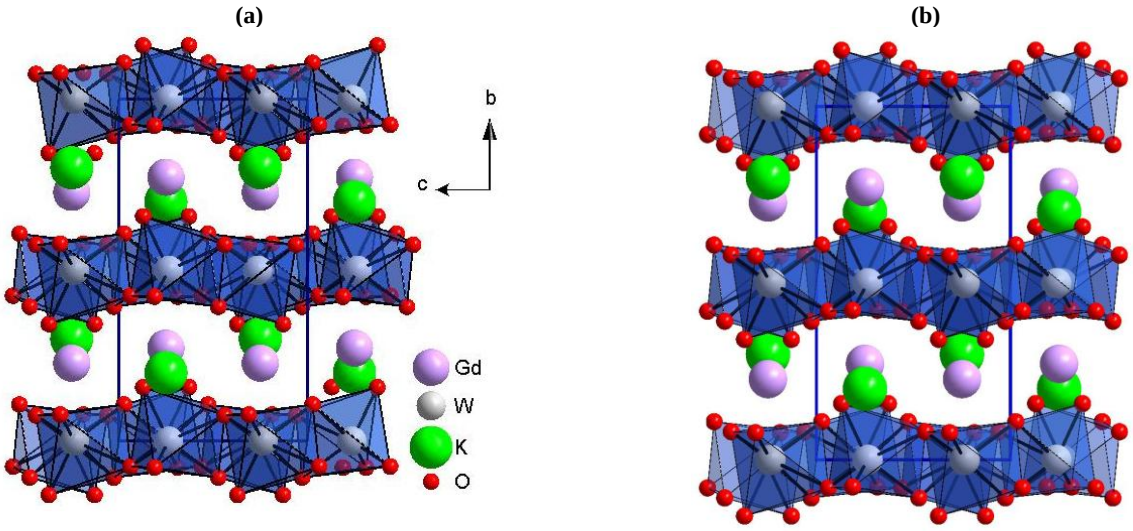

Figure 1. Crystal structure projection of KGW along *a* axis at RT (a) and 11 K (b).

[001] (*z* direction) and to [010] (*y* direction). The 1064 nm line of YAG:Nd laser was used as an excitation. Signal detection was performed with the LN-Ge (D418-T) liquid nitrogen-cooled NIR detector with an integrated preamplifier and high voltage power supply. The spectral resolution was 2 cm^{-1}. The temperature-dependent spectra were measured using a helium-flow Oxford cryostat.

3. Crystal structure

The low-temperature phase of the potassium gadolinium tungstate is monoclinic with C2/c space group. It comprises four chemical formula units per unit cell with the lattice parameters being almost the same as of Pujol et al. [8]: *a* = 10.683(2) Å, *b* = 10.452(2) Å, *c* = 7.583(2) Å and β = 130.70(3)°. The crystal structure projections along a and c axes are presented in Figure 1 and 2, respectively, for RT and 11 K (a and b, respectively). The crystal data, experimental details and the structure refinement parameters are listed in Table 1. To confro the crystallographic data with the EPR measurements where some temperature dependencies have been found, the single crystal diffraction analysis was additionally performed at 11 K. It is seen from the Table 1 that there are not any structural changes up to low temperature.

The results of refined crystal structures at RT and 11 K are presented in Table 2 and the selected bond lengths and

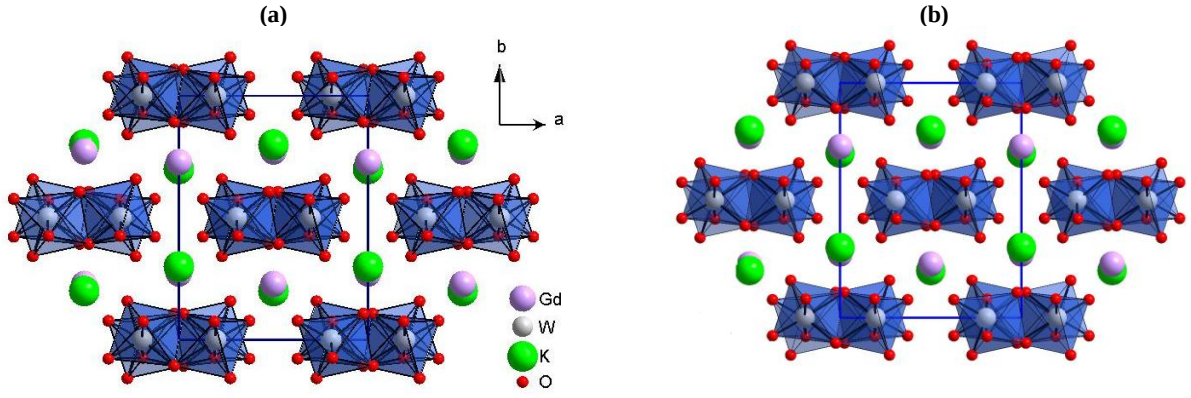

Figure 2. Crystal structure projection of KGW along *c* axis at RT (a) and 11 K (b).

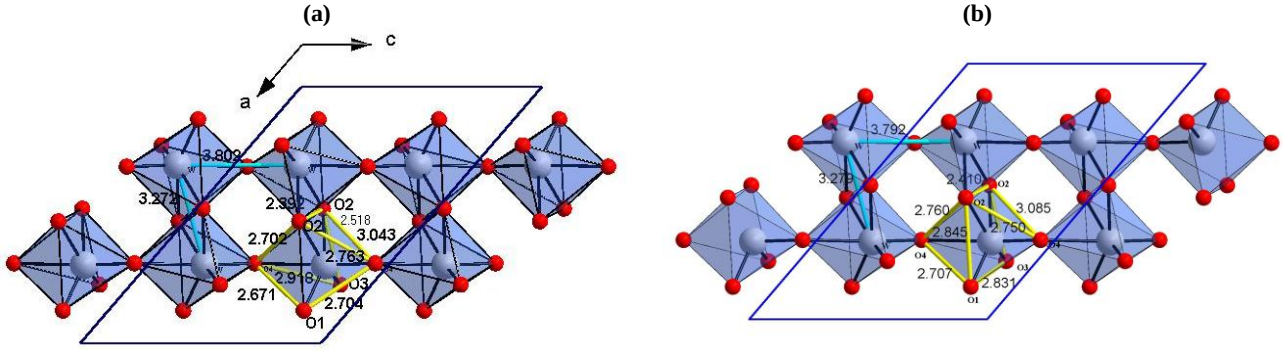

Figure 3. Double chains formed by tungstate octahedra at RT (a) and 11 K (b) in monoclinic phase of $KGd(WO_4)_2$ crystal.

Table 2. Atomic coordinates (x 10^4) and equivalent isotropic displacement parameters ($Å^2$ x 10^3) for $KGd(WO_4)_2$ at RT and 11 K. *U*(eq) is defined as one third of the trace of the orthogonalized U_{ij} tensor.

11 K	**x**	**y**	**z**	***U*(eq)**
Gd	0	7284(1)	2500	10(1)
W	1953(1)	1(1)	7363(1)	10(1)
K	5000	2011(3)	7500	15(1)
O(1)	3727(5)	-768(6)	8141(8)	10(2)
O(2)	-243(6)	1079(6)	5271(9)	16(2)
O(3)	2722(6)	1590(6)	8706(9)	15(2)
O(4)	1898(6)	-796(6)	9392(8)	12(2)
RT	x	y	z	*U*(eq)
Gd	0	7281(1)	2500	3(1)
W	1949(1)	-1(1)	7359(1)	3(1)
K	5000	2001(2)	7500	14(1)
O(1)	3725(5)	-776(4)	8114(8)	9(1)
O(2)	-248(5)	1069(4)	5272(7)	6(1)
O(3)	2717(5)	1577(4)	8709(7)	7(1)
O(4)	1884(5)	-745(4)	9389(8)	7(1)

angles are listed in Table 3. Determination of the crystal structure at RT and 11 K confirmed that the structures are isostructural. The atomic parameters and interatomic distances are well comparable with the data performed by Pujol et al. [8]. The structural motif consists of WO_6 tungstate-oxygen octahedrons linking by the common edges. The chains presented in Figures 1 and 2 are constituted and they are extended along *c* axis at which cavities creates occupied by the K and Gd atoms. The changes of the important distances of the distorted octahedra, i.e. W–W, W–O and O–O, at 11 K in comparison to the room temperature are not large (see Figure 3).

4. Raman spectra

Raman spectroscopy is known to be powerful probe for understanding details of structural changes and spin-phonon and crystal-field-phonon interactions in magnetic and ferroelectric materials [10, 11]. Previously we reported the data on phonon properties of $KGd(WO_4)_2$ single crystal based on normal coordinate analysis and potential energy distribution [7]. The present experiment was focused on phonon behaviour with decrease of temperature. Temperature-dependent Raman studies were performed from room down to liquid helium temperature. Raman spectra of KGW single crystal measured in *ab* plane at selected temperatures are shown in Figure 4.

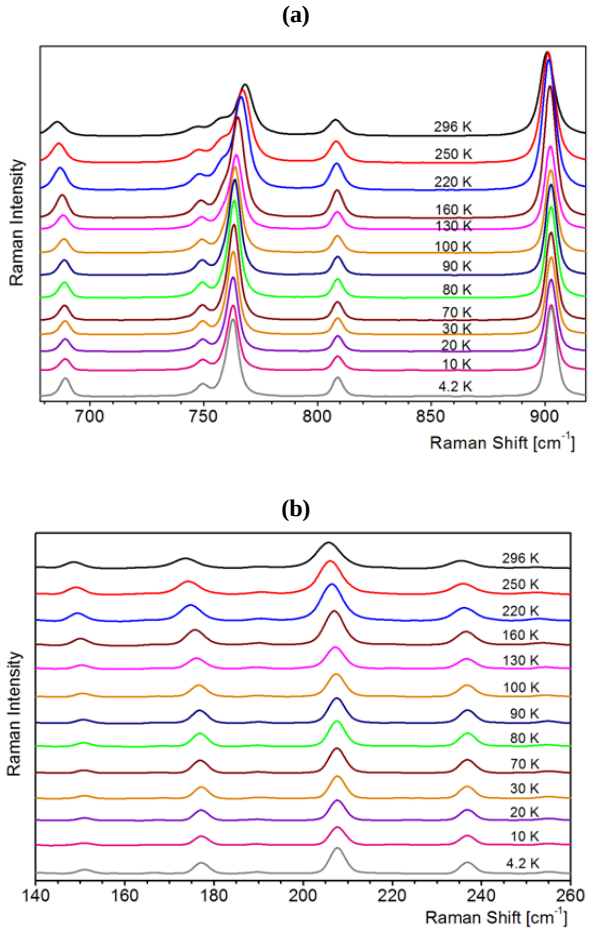

Figure 4. Temperature dependence of frequency of the high-energy modes at 685, 768 and 901 cm^{-1} (a) and lattice vibrations at 235, 206, 173 and 148 cm^{-1} (b). Raman spectra of KGW single crystal in *ab* plane were measured at selected temperatures.

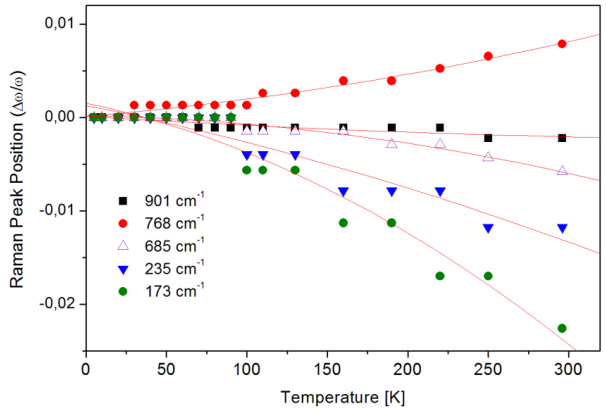

Figure 5. Relative thermal evolution of the peak position of selected Raman modes of KGW.

They remain qualitatively the same up to 4 K apart from the chosen plane. Any appearance nor disappearance of some Raman bands neither splitting of the bands is observed with the decrease of temperature. We have not found any evidence on structural changes of KGW crystal along the temperature range. Nevertheless, Raman spectra show some not very significant shifts of Raman peaks as the temperature is decreased. Internal modes located at 901 cm^{-1} and 685 cm^{-1} [7] are slightly shifted to higher wavenumbers. In the range of lattice modes the small shifts of Raman modes located at 148, 173, 206 or 235 cm^{-1} are observed. All peaks show an increase of wavenumber when the temperature decreases. On the other hand, a monotonic shift of 768 cm^{-1} mode towards lower wavenumbers is observed up to 100 K. The temperature dependence ($\Delta\omega/\omega$) of wavenumbers of the chosen vibration modes of KGW is shown in Figure 5. The wavenumber change ($\Delta\omega$) between T (300 - 4 K) is divided by the wavenumber (ω) at T for each mode.

The temperature shift of vibronic frequency was observed in different materials [12-14]. The temperature dependence arises from two processes. The first one is due to the thermal expansion of the lattice that leads to the downshift of the phonon frequency with heating the sample. Decrease of the an harmonic thermal motion should also make the line widths of phonons narrower [14]. The second process, usually weaker, is determined by the effects of the an harmonic terms in the thermal expansion in terms of displacement. It results with increase of phonon frequency with increasing temperature [12]. Upon cooling, almost all modes listed above show conventional tendency, an anomaly is observed for 768 cm^{-1} where phonon energy is decreased with decreasing temperature. The line width of all phonon bands become narrower as usual. For the phonon modes around 901, 685, 235, 206, 173 and 148 cm^{-1} their temperature dependencies could be explained in terms of the usual thermal effect. The temperature dependency of the 768 cm^{-1} mode could not be simply explained in this way.

This effect can be explained using the results of polarized Raman spectra measurement performed for $KGd(WO_4)_2$ and $KY(WO_4)_2$ single crystals in our previous papers [7, 15]. The assignment of the phonon bands to the respective vibrational normal modes was there made on the basis of theoretical calculations in which the inter-molecular interactions of the W^OW and $W^O{}_OW$ type between the tungstate octahedra have been taken into account. These calculations clearly showed that the Raman band at 768 cm^{-1} corresponds to the stretching vibration of the $W^O{}_OW$ double oxygen bond system. It was also reported that the vibrational modes of such type play an important role in the electron-phonon coupling and, consequently, in the energy transfer in the studied crystals [15]. Such interactions are facilitated due to the very short distance between the Gd^{3+} ions and the O(2) oxygen atoms engaged in the double oxygen bond (2.307 Å at room temperature). This distance is the shortest among all gadolinium-oxygen bond lengths in the unit cell (see Table 3).

5. EPR measurements

Figure 6 shows the EPR spectra (first derivative of the absorption) of KGW single crystal measured at several temperatures. All the spectra were recorded at the same position of rotation angle of investigated sample, when magnetic filed (***B***) lied in the ***bc*** – crystallographic plane. The temperature varied from 20,4 K (top line) down to 6 K (bottom line). The unit cell of the yttrium monoclinic tungstate doped with gadolinium contains four yttrium ions. Each Y ion can be substituted by a Gd ion. All four ions occupy positions on the C_2-axis and are equivalent. Therefore, a single EPR spectrum is expected to be observed in the EPR experiments [16]. In case of KGW crystal the EPR lines (Figure 6a) are very broad and have a complex shape. Moreover, as it can be seen, EPR signal is observed even over 850 mT, what is not

Table 3. Bond lengths (Å) and angles (deg.) for $KGd(WO_4)_2$ at RT and 11 K.

11 K				RT			
Gd-O(2)#1	2.297(7)	K-O(4)#12	2.762(6)	Gd-O(2)#1	2.307(5)	K-O(4)#12	2.807(5)
Gd-O(2)#2	2.297(7)	K-O(4)#6	2.762(6)	Gd-O(2)#2	2.307(5)	K-O(4)#6	2.807(5)
Gd-O(1)#3	2.336(7)	K-O(4)#9	2.823(5)	Gd-O(1)#3	2.319(4)	K-O(4)#9	2.850(5)
Gd-O(1)#4	2.336(7)	K-O(4)#10	2.823(5)	Gd-O(1)#4	2.319(4)	K-O(4)#10	2.850(4)
Gd-O(3)#5	2.365(5)	K-O(1)#9	2.933(6)	Gd-O(3)#5	2.370(4)	K-O(1)#9	2.946(5)
Gd-O(3)#6	2.365(5)	K-O(1)#10	2.933(6)	Gd-O(3)#6	2.370(4)	K-O(1)#10	2.946(5)
Gd-O(3)#2	2.685(7)	K-O(2)#13	3.029(7)	Gd-O(3)#2	2.687(4)	K-O(2)#13	3.050(5)
Gd-O(3)#1	2.685(7)	K-O(2)#4	3.029(7)	Gd-O(3)#1	2.687(4)	K-O(2)#4	3.050(5)
		K-O(3)	3.139(8)			K-O(3)	3.152(5)
Gd-W#2	3.5636(8)	K-O(3)#14	3.139(8)	Gd-W#2	3.5659(5)	K-O(3)#14	3.152(5)
Gd-W#1	3.5636(8)	K-O(1)#14	3.375(7)	Gd-W#1	3.5659(5)	K-O(1)	3.364(5)
Gd-K#5	3.8023(10)	K-O(1)	3.375(7)	Gd-K#7	3.8130(5)	K-O(1)#14	3.364(5)
Gd-K#7	3.8023(10)			Gd-K#5	3.8130(5)		
		O(1)-Gd#4	2.336(7)			O(1)-Gd#4	2.319(4)
W-O(1)	1.769(6)	O(1)-K#10	2.933(6)	W-O(4)	1.769(5)	O(1)-K#10	2.946(5)
W-O(4)	1.784(7)	O(2)-W#8	1.960(5)	W-O(1)	1.780(4)	O(2)-W#8	1.949(4)
W-O(3)	1.839(6)	O(2)-Gd#1	2.297(7)	W-O(3)	1.828(4)	O(2)-Gd#1	2.307(5)
W-O(2)#8	1.960(5)	O(2)-K#4	3.029(7)	W-O(2)#8	1.949(4)	O(2)-K#4	3.050(5)
W-O(2)	2.107(5)	O(3)-Gd#15	2.365(5)	W-O(2)	2.101(4)	O(3)-Gd#15	2.370(4)
W-O(4)#9	2.366(7)	O(3)-Gd#1	2.685(7)	W-O(4)#9	2.347(5)	O(3)-Gd#1	2.687(4)
		O(4)-W#16	2.366(7)			O(4)-W#16	2.347(5)
W-Gd#1	3.5636(8)	O(4)-K#11	2.762(6)	W-Gd#1	3.5659(5)	O(4)-K#11	2.807(5)
W-K#10	3.695(2)	O(4)-K#10	2.823(5)	W-K#10	3.6913(18)	O(4)-K#10	2.850(4)
W-K#11	3.796(2)			W-K#11	3.801(2)		
W-K	3.8188(16)			W-K	3.8175(15)		

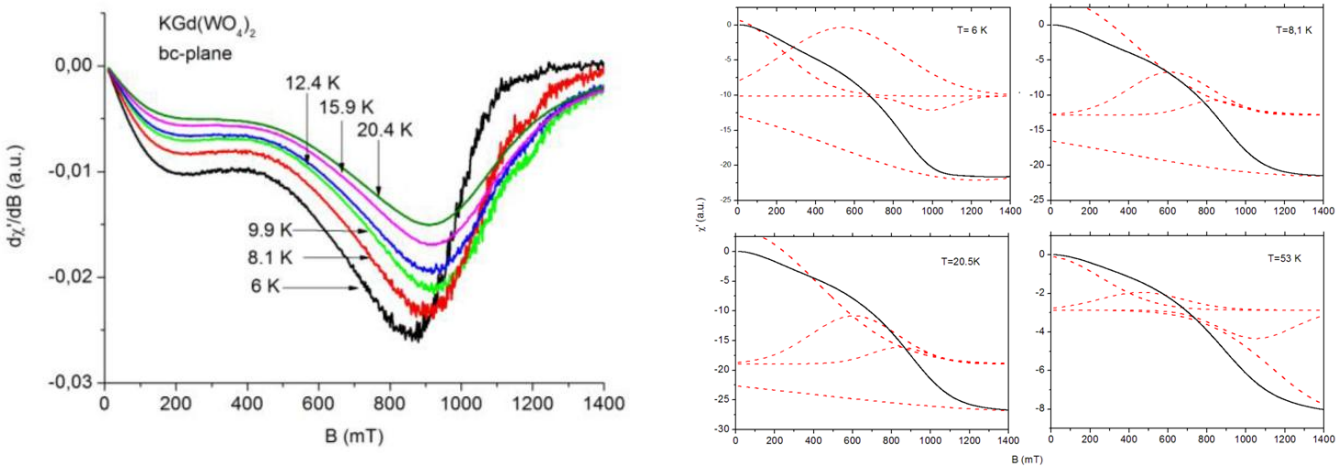

Figure 6. a). EPR spectra of $KGd(WO_4)_2$ single crystal recorded at six different temperatures, b). Decomposition of some of the spectra (EPR absorption) into four components derived using Origin standards.

usual remark. Due to its broadening we can imply that in this range of magnetic field clear signal from gadolinium pairs of ions is observed. In Figure 6b decomposition into four components of Gaussian type of some EPR lines measured for different temperatures between 6 and 54 K is presented. Changes in a shape, width and height of the EPR resonance lines are clearly visible when temperature decreases. The shape of the constituent lines indicates on dipole-dipole magnetic interactions prevailing in the KGW system.

The spectra in Figure 6a were chosen to see temperature dependence of the EPR signal in low temperature range, where we previously observed unusual behaviour of the temperature dependence of total intensity of EPR spectrum [17]. The total intensity was calculated by integration of the EPR absorption spectrum or as a double integral of the EPR spectrum (EPR susceptibility). The full analysis of the temperature dependence of EPR spectra was reported elsewhere [17]. The analysis of the total intensity and the inverse of the total intensity of the EPR spectra have shown that there are two temperatures, first one at 66.8 ± 3.3 K and the second one at 9.9 ± 2.8 K, when the total intensity considerably changes. We suggested that some kind of rearrangements in the mutual positions of gadolinium ions, as an effect of, e.g., impairment of magnetic interactions between

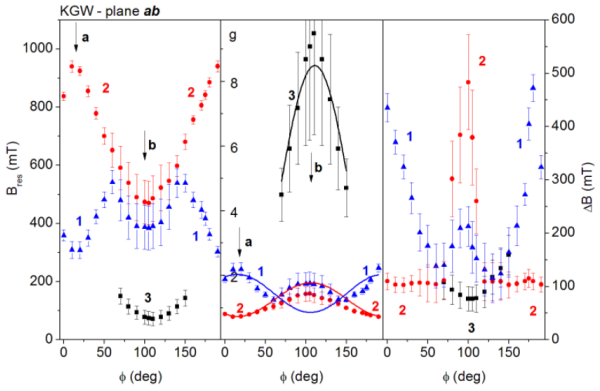

Figure 7. Angular dependences of the resonance EPR line position, B_{res}, g-factor, and, linewidth, ΔB; sample rotation in ***ab***-plane at 10.6 K.

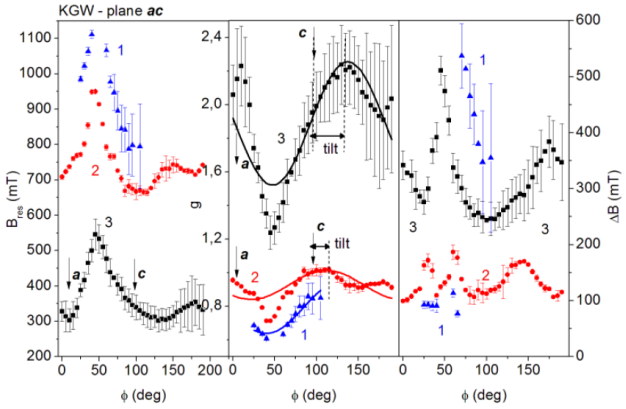

Figure 8. Angular dependences of the resonance EPR lines position, B_{res}, g-factor, and, linewidth, ΔB; sample rotation in ***ac***-plane at 10.6 K.

ions within chains or planes, may be responsible for high temperature changes (at e.g. 66.8 K) observed in EPR spectra [17] .

The analysis performed in [17] was based on a classical character of magnetic interactions dominating a shape of the EPR spectra, i.e. Lorentzian like and Gaussian like (exchange or dipole-dipole magnetic interactions). Borowiec et al. have claimed that comparison between magnetic measurements of KGW crystal with those obtained in EPR measurements of $KY(WO_4)$:Gd^{3+} crystals is justified because the diluted $KY(WO_4)_2$ crystal is isomorphic with KGW [18]. In concentrated magnetic system however, to which belongs $KGd(WO_4)_2$, the shape of the EPR spectra should be ascribed by more complex function as e.g. given by Dyson [19]. We predicted at least three asymmetric lines to which one can decompose the EPR spectra using a relation [20]:

$$\frac{d}{dB}P_{abs} \approx \frac{d}{dB}\sum_i \left(\frac{\Delta B + \alpha(B - B_{res})}{(B - B_{res})^2 + \Delta B^2} + \frac{\Delta B + \alpha(B + B_{res})}{(B + B_{res})^2 + \Delta B^2} \right) \quad (1)$$

where B – applied magnetic induction, α describes the asymmetry of EPR line (anisotropy factor). P_{abs} is the power absorbed in the EPR experiment, B_{res} is a resonance

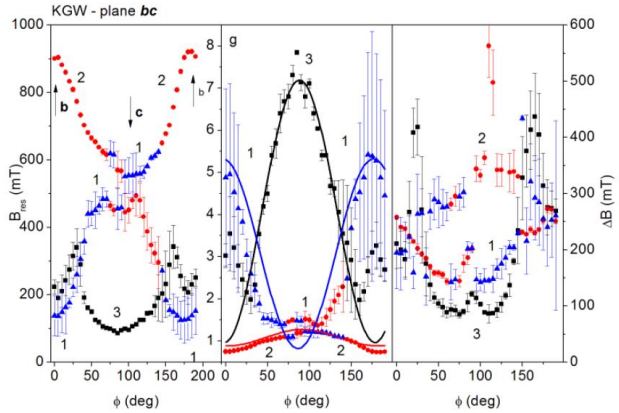

Figure 9. Angular dependences of the resonance EPR lines position, B_{res}, g-factor, and, linewidth, ΔB; rotation in ***bc***-plane at 10.6 K.

magnetic field, ΔB is a linewidth, α<1 represents an asymmetry parameter describing an admixture of dispersion, and, the index i refers to the i-th line. Such asymmetric lineshapes are usually observed in metals, because of skin effect [19]. A second reason for the asymmetry arises from the influence of non diagonal elements of the dynamic susceptibility, that are characteristic for low symmetry magnets [20, 21]. Due to the large linewidth we took into account both circular components of the line at $+B$ and $-B$, respectively.

Figures 7, 8 and 9 show the full angular dependences of the resonance field, g-factor and a linewidth calculated in a temperature of 10,6 K for ***ab***, ***bc*** and ***ac*** planes, respectively. For all calculated points error bars were found and drawn. The angular dependences reveal low, C_2, local symmetry of gadolinium centres in KGW single crystal. One can see some deviations of extremes of the curves from crystallographic axes are observed, e.g. in ***ac*** plane. They are different for each of three lines. The lines could be assigned to three different kinds of magnetic centers in KGW crystal of which two lines (No. 1, 2 in Figures 7a-9a), appearing in larger values of magnetic resonance fields, are responsible for complex centers of Gd^{3+} ions. Angular dependences of g-factors were analyzed using a standard relation:

$$g^2 = g_1^2 \cos^2(\theta + \delta) + g_2^2 \sin^2(\theta + \delta) \quad (2)$$

where θ represents an angle between the magnetic field and crystallographic axis, δ is a tilting angle between a local symmetry axis and a crystallographic axis and $g_{1,2}$ represents extreme values of g-factors in a given plane. The fitting to Eq. (2) enabled a quantitative description of selected resonances (Table 4). The analysis in the ***ac*** plane suggests a tilting of local symmetry axes by about 42.6° with respect to the c-axis for one of the three centers, and 21.4° for the second one (see Table 4). We could not find the tilting for third center due to too large calculation error.

In Figures 10-12 temperature dependence of the resonance line position, linewidth and anisotropy parameter α are presented for two of the three above mentioned lines (see Table 4). In the figures error bars are also presented. One can recognize two characteristic temperatures from the figures: ~10K and ~67 K. These are very similar temperatures as reported in [17]. At a temperature of ~10 K one can observe

Table 4. *g*-factor parameters of the three gadolinium centers.

g-factor	Center No 1	Center No 2	Center No 3
g_x	1.86	0.71	1.86
g_y	0.85	1.77	7.83
g_z	0.82	1.28	7.18
tilt	-	21.4°	42.6°

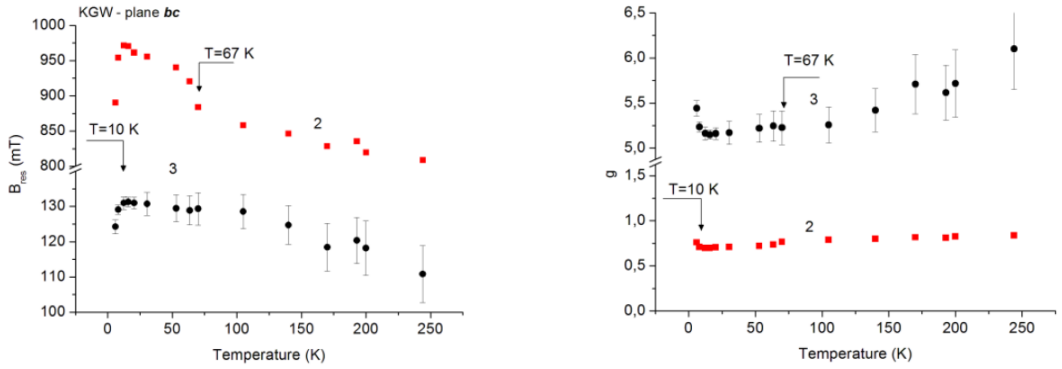

Figure 10. Temperature dependence of a). resonance magnetic field, B_{res}, b). *g*-factor (g=0,0000007144775*9,46*10^9/B_{res}) in ***bc***-plane for two of three centers numbered in Table 4.

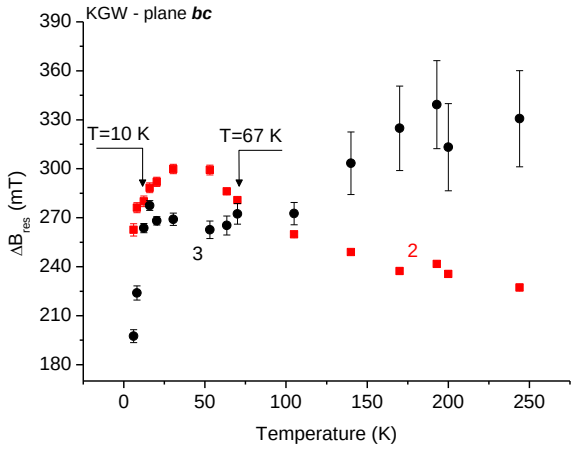

Figure 11. Temperature dependence of EPR linewidth, ΔB_{res} (mT), in ***bc***-plane for two of three lines numbered in Table 4.

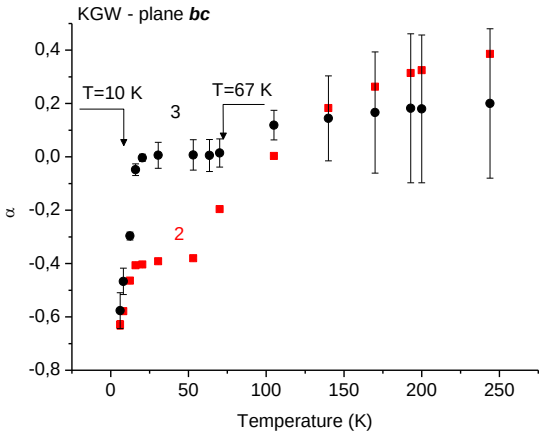

Figure 12. Temperature dependence of anisotropy factor, α, in ***bc***-plane for two of three lines numbered in Table 4.

sudden increase in a value of resonance magnetic field, linewidth and anisotropy parameter suggesting some kind of magnetic phase transition or strong change in a magnetic ordering between gadolinium ions. Similar conclusion was derived from analysis of the same crystal using approximation of dilute magnetic system [17]. At a temperature of ~67 K a change in an inclination of temperature dependence of both, resonance filed and linewidth, is observed. Moreover increasing of an anisotropy parameter over 0 could be observed. It suggests that some kind of rearrangement of magnetic entities takes place, influencing strength of antiferromagnetic interactions. Previously we reported impairment of gadolinium antiferromagnetic interactions at the temperature [17]. The two lines seen in Figures 11, 12 may be also a result of two at least different distances between gadolinium ions in KGW matrix. The distance between two nearest Gd^{3+} ions is equal to 4.0701(19) Å [8]. There are four Gd^{3+} ions in such distances forming a chain. The ions within a chain may easily interact. Similarly, Gd^{3+} ions interacting via O^{2-} oxygen bridges may form magnetically inequivalent structures, from pairs of Gd^{3+} - Gd^{3+} ions to various clusters of Gd^{3+} ions.

To find confirmation on the origin of the above mentioned paramagnetic centers we tried to fit angular dependencies presented in Figures 7-9 applying EPR-NMR program [22] and spin Hamiltonian in the following form:

$$H = g_0\mu_B B \cdot S + \sum_{m=-l}^{l} B_l^m \cdot O_l^m(S) \qquad (3)$$

where the first term is the electronic Zeeman term, the second one contains the higher order (l=2,4,6) Stevens parameters. Other symbols have got their usual meaning.

The results of this fitting is shown in Figures 13-15. Basing on this fitting we derived spin Hamiltonian parameters gathered in Table 5a, b. As one can see two centers we have found: isolated gadolinium ions and pairs of gadolinium ions,

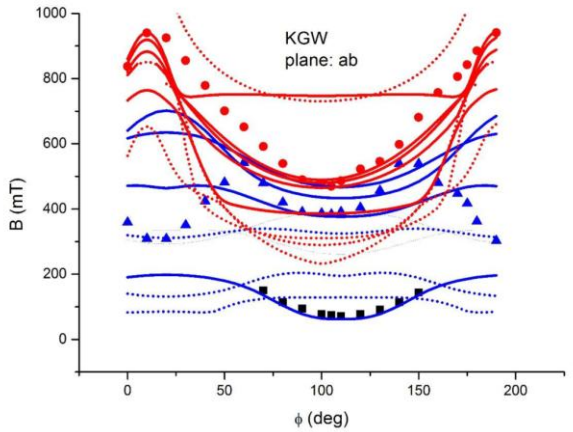

Figure 13. Angular dependences of the resonance EPR line positions and fitting curves obtained according to eq. (3) in *ab* plane. Blue solid lines are fitted lines for isolated centers, dotted blue lines are calculated lines for the centers. Red lines are fitted lines for paired centers, dotted red lines are calculated lines for the centers.

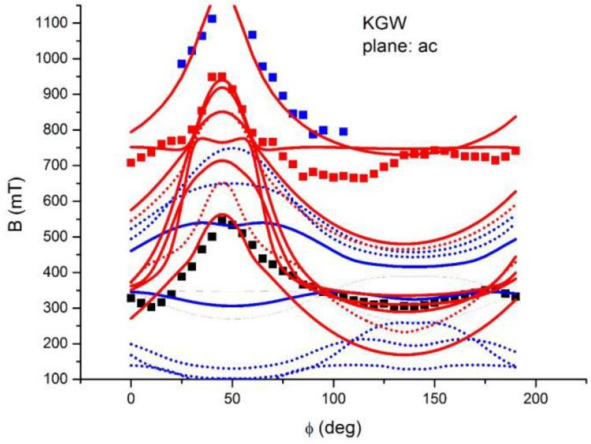

Figure 14. Angular dependences of the resonance EPR line position and fitting curves obtained according to eq. (3) in *ac* plane. Blue solid lines are fitted lines for isolated centers, dotted blue lines are calculated lines for the centers. Red lines are fitted lines for paired centers, dotted red lines are calculated lines for the centers.

very similarly as we reported previously [17]. As one can see spin Hamiltonian parameters are typical for Gd ions in $KGd(WO_4)_2$ matrix.

6. Discussion and conclusions

The structural and magnetic properties of the $KGd(WO_4)_2$ single crystal were investigated using the XRD, EPR and Raman techniques. The crystallographic measurements prove that the low-temperature phase of double potassium gadolinium tungstate is monoclinic with C2/c space group and remains unchanged up to 11 K. Temperature-dependent Raman studies show phonon frequency shifts that could be explained by phonon-phonon anharmonic interaction, whereas anomaly behaviour of the phonon mode around 768 cm^{-1} could be presumably attributed to very weak spin-phonon coupling.

Results obtained from the EPR measurements may suggest, that several magnetically different systems are present in the KGW single crystal. These magnetic systems may be assigned to different kinds of magnetic interactions between Gd^{3+} ions, e.g. isolated or paired Gd^{3+} ions.

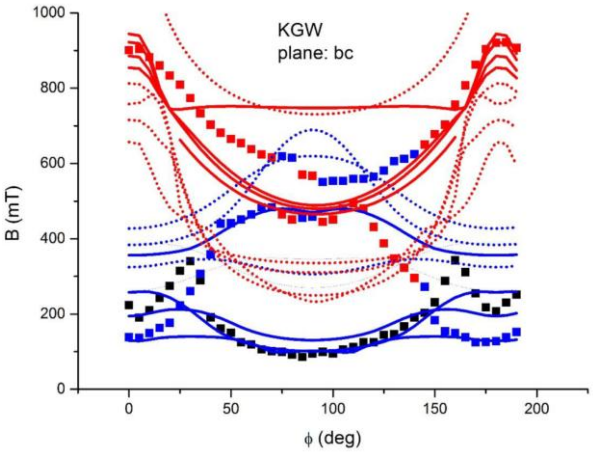

Figure 15. Angular dependences of the resonance EPR line position and fitting curves obtained according to eq. (3) in *bc* plane. Blue solid lines are fitted lines for isolated centers, dotted blue lines are calculated lines for the centers. Red lines are fitted lines for paired centers, dotted red lines are calculated lines for the centers.

Individual systems may determine the behaviour of the EPR spectra in different temperature ranges. We found three ranges of linear change: first one up to ~10 K, the second one from 10 to ~67 K and the third one from ~67 K to 250 K. Two limiting temperatures, first one at ~67 K and the second one at ~10 K were observed. We could explain this behaviour by assuming that at these temperatures we are dealt with a change in a kind of dominating magnetic interactions or different magnetic systems, e.g. inter chains, intra chains and pairs or clusters. Such conclusion confirms Raman data [7, 9] where between 450 and 750 cm^{-1} specific bands assigned to stretching modes of the $W^{O}W$ and $W^{O}{}_{O}W$ oxygen bonds are observed. Such single and double oxygen bridges could be a source of complex magnetic behaviour between gadolinium ions in $KGd(WO_4)_2$ with polymeric structure.

As compared to diluted $KY(WO_4)_2$:Gd system, in KGW EPR spectrum one cannot distinguish its fine structure, because measured EPR spectrum of dense magnetic system may be a superposition of all signals originating from the fine structure of magnetically inequivalent paramagnetic isolated Gd^{3+} ions or more complex gadolinium centers . Its asymmetric shape allowed us to decompose the spectrum onto three lines, each having different tilt angle with respect to the *c*-axis. Analysis performed in [17], when KGW was treated as diluted medium, has given also three different centers one of which was isolated Gd^{3+} center and two other were Gd-Gd pairs centers. Calculated in this paper spin Hamiltonian parameters were typical for gadolinium ions. Presented in Table 4 *g*-factors are not calculated from the spin Hamiltonian analysis and differ from typical values expected for gadolinium ions. This difference results from dense magnetic state of KGW crystal. Real magnetic interactions in KGW dense magnetic medium differ significantly from predicted by spin Hamiltonian analysis performed for diluted system. Spin Hamiltonian analysis in [17] was based on fittings of a spin Hamiltonian to angular dependencies obtained by taking into account only exchange or dipole-dipole magnetic interactions. In concentrated magnetic systems magnetic interactions are more complex. We have performed analysis of the influence of Gd^{3+} increasing concentration on kind of magnetic interactions in $KY(WO_4)_2$:Gd powders [23]. From the analysis

Table 5. Elements of g and B_l^m matrices calculated using EPR-NMR program for $KGd(WO_4)_2$ single crystal: a). isolated Gd centers, b). pairs of Gd ions.

(a)

Isolated Gd centers
$g = \begin{bmatrix} 2.02 & & \\ & 2.06 & \\ & & 2.15 \end{bmatrix}$
$B_2^0 = 292(10) \cdot 10^{-4}\ cm^{-1}$ $B_2^2 = -316(12) \cdot 10^{-4}\ cm^{-1}$
$B_4^0 = 2.4(2) \cdot 10^{-4}\ cm^{-1}$ $B_4^2 = 1.8(2) \cdot 10^{-4}\ cm^{-1}$ $B_4^4 = 1.5(2) \cdot 10^{-4}\ cm^{-1}$ $B_4^{-2} = 2.2(2) \cdot 10^{-4}\ cm^{-1}$
$B_6^0 = -2.20(5) \cdot 10^{-4}\ cm^{-1}$ $B_6^2 = -1.5(2) \cdot 10^{-4}\ cm^{-1}$ $B_6^4 = 0.3(1) \cdot 10^{-4}\ cm^{-1}$ $B_6^{-2} = 1.1(3) \cdot 10^{-4}\ cm^{-1}$ $B_6^{-4} = 2.0(2) \cdot 10^{-4}\ cm^{-1}$

(b)

Pairs of Gd ions
$g = \begin{bmatrix} 1.71 & & \\ & 1.89 & \\ & & 1.92 \end{bmatrix}$
$B_2^0 = 290(10) \cdot 10^{-4}\ cm^{-1}$ $B_2^2 = -346(10) \cdot 10^{-4}\ cm^{-1}$
$B_4^0 = 1.8(2) \cdot 10^{-4}\ cm^{-1}$ $B_4^2 = 1.6(2) \cdot 10^{-4}\ cm^{-1}$ $B_4^4 = 1.5(2) \cdot 10^{-4}\ cm^{-1}$ $B_4^{-2} = 2.0(2) \cdot 10^{-4}\ cm^{-1}$
$B_6^0 = -1.75(5) \cdot 10^{-4}\ cm^{-1}$ $B_6^2 = -1.5(2) \cdot 10^{-4}\ cm^{-1}$ $B_6^4 = 0.3(1) \cdot 10^{-4}\ cm^{-1}$ $B_6^{-2} = 0.1(1) \cdot 10^{-4}\ cm^{-1}$ $B_6^{-4} = 2.0(2) \cdot 10^{-4}\ cm^{-1}$

we have found that the investigated powder samples have shown basically antiferromagnetic kind of magnetic interactions between gadolinium ions (similarly, as in the case of KGW single crystal) but the strength of these interactions was different and depended on the gadolinium concentration and a temperature. Not all of conclusions made in the paper could be adopted to the present paper, because EPR measurements of powder samples were performed at temperatures higher than 80 K. Nevertheless, temperature dependence of a strength of magnetic interactions due to e.g. presence of internal magnetic fields (intra chains or inter chains or planes interactions) may occur in KGW crystals. In the paper we confirmed general conclusions resulting from [17] and [23] but adopting other kind of decomposition lines for EPR spectrum, we have obtained more realistic description of magnetic interactions in dense KGW magnetic system. The studies of the KGW are of scientific interest also because of its magnetic behavior peculiarities at ultralow temperatures. Recently typical second order magnetic phase transition was reported for KGW crystal at T=0.42 K, but analyzing the specific heat investigations [24]. EPR and magnetic susceptibility measurements are not effective in such a case.

References

1. A. A. Kaminskii, Ann Phys Fr 16 (1991) 639.
2. M. C. Pujol, M. Aguilo, F. Diaz and C. Zaldo, Opt. Mater. 13 (1999) 33.
3. T. Graf and J. E. Balmer, Opt. Eng. 34 (1995) 2349.
4. T. T. Basiev, A. A. Sobol, P. G. Zverev, L. I. Ivleva, V. V. Osiko and R. C. Powell, Opt. Mater. 11 (1999) 307.
5. P. G. Zverev, T. T. Basiev and A. M Prokhorov, Opt. Mater. 11 (1999) 335.
6. A. S. Kumaran, A. L. Chandru, S. M. Babu, I. Bhaumik, S. Ganesamoorthy, A. K. Karnal, V. K. Wadhawan and M. Ichimura, J. Cryst. Growth 275 (2005) e2117.
7. L. Macalik, J. Hanuza and A. A. Kaminskii, J. Raman Spectrosc. 33 (2002) 92.
8. M. C. Pujol, R. Sole, J. Massons, Jna. Gavalda, X. Solans, C. Zaldo, F. Diaz and M. Aguilo, J. Appl. Crystallogr. 34 (2001) 1.
9. G. M. Sheldrick, Acta Crystallogr. A 64 (2008) 112.
10. A. F. García-Flores, E. Granado, H. Martinho, R. R. Urbano, C. Rettori, E. I. Golovenchits, V. A. Sanina, S. B. Oseroff, S. Park, S.-W. Cheong, Phys. Rev. B 73 (2006) 104411.
11. M. Ptak, M. Mączka, A. Pikul, P. E. Tomaszewski, J. Hanuza, J. Solid State Chem. 212 (2014) 218.
12. P. G. Zverev, T. T. Basiev, V. V. Osiko, A. M. Kulkov, V. N. Voitsekhovskii and V. E. Yakobson, Opt. Mater. 11 (1999) 315.
13. J. Kalus, J Chim Phys Physchim Biol 82 (1985) 137.
14. M. Balkanski, R. F. Wallis and E. Haro, Phys. Rev. B 28 (1983) 1928.
15. L. Macalik, J. Hanuza and A. A. Kaminskii, J. Mol. Struct. 555 (2000) 289.
16. M. T. Borowiec, V. Dyakonov, V. Kamenev, I. Krygin, S. Piechota, A. Prokhorov, and H. Szymczak, Phys. Status Solidi B 209 (1998) 443.
17. S. M. Kaczmarek, G. Leniec, T. Bodziony, H. Fuks, T. Skibiński, J. Hanuza, L. Macalik, J Mater Sci Res 2 (2013) 23.
18. M. T. Borowiec, T. Zayarnyuk, M. C. Pujol, M. Aguilo, F. Diaz, E. E. Zubov, A. D. Prokhorov, M. Berkowski, W. Domuchowski, A. Wisniewski, R. Puzniak, J. Pietosa, V. P. Dyakonov, M. Baranski, H. Szymczak, Physica B 405 (2010) 4886.
19. F. J. Dyson, Phys. Rev. 98 (1955) 349.
20. H. Benner, M. Brodehl, H. Seitz and J. Wiese, J Phys C 16 (1983) 6011.
21. J. Choukroun, J.-L. Richard. and A. Stepanov, Phys. Rev. B 68 (2003) 144415.
22. Mombourquette, M. J., Weil, J. A., & McGavin, D. G., EPR-NMR User's Manual, Department of Chemistry, University of Saskatchewan, Saskatoon, SK, Canada (1999).
23. G. Leniec, L. Macalik, S. M. Kaczmarek, T. Skibiński, J. Hanuza, J. Mater. Res. 27 (2012) 2973.
24. M. T. Borowiec, T. Zayarnyuk, M. U. Gutowska, J. Wieckowski, A. Szewczyk, V. Dyakonov, E. Zubov, M. Baranski, V. Domukhovski, M. C. Pujol, M. Aguiló, F. Díaz, H. Szymczak, Cent. Eur. J. Phys. 11 (2013) 394.

Cite this article as:

L. Macalik Lin *et al.*: **Temperature behaviour of the structural, magnetic and vibrational properties of $KGd(WO_4)_2$ single crystal.** ScienceJet 2015, **4**: 122